INCREMENTS IN AEROFOIL LIFT COEFFICIENT AT ZERO ANGLE OF ATTACK AND IN MAXIMUM LIFT COEFFICIENT DUE TO DEPLOYMENT OF VARIOUS LEADING-EDGE HIGH-LIFT DEVICES AT LOW SPEEDS

1. NOTATION AND UNITS

		SI	*British*
a_l	theoretical rate of change of lift coefficient with leading-edge device deflection, Equation (3.3)	rad^{-1}	rad^{-1}
a_{ml}	theoretical rate of change of maximum lift coefficient with leading-edge device deflection, Equation (3.9)	rad^{-1}	rad^{-1}
C_{Lm}	maximum lift coefficient of aerofoil with high-lift devices deployed, based on c		
C_{L0}	lift coefficient at zero angle of attack for aerofoil with high-lift devices deployed, based on c		
ΔC_{Lml}	increment in maximum lift coefficient due to deployment of leading-edge device, based on c, Equation (3.12)		
$\Delta C'_{Lml}$	increment in maximum lift coefficient due to deployment of leading-edge device, based on c', Equation (3.8) or (3.10), at datum Reynolds number $R_c = 3.5 \times 10^6$		
ΔC_{L0l}	increment in lift coefficient at zero angle of attack due to deployment of leading-edge device, based on c, Equation (3.7)		
$\Delta C'_{L0l}$	increment in lift coefficient at zero angle of attack due to deployment of leading-edge device, based on c', Equation (3.6)		
$[\Delta C'_{L0l}]_1$	contribution to $\Delta C'_{L0l}$ dependent on leading-edge device type and deflection, Equation (3.2)		
$[\Delta C'_{L0l}]_2$	contribution to $\Delta C'_{L0l}$ dependent on leading-edge device type, see Table 4.1		
c	basic (plain) aerofoil chord (*i.e.* chord with high-lift devices undeployed), see Sketch 4.1	m	ft
c'	extended aerofoil chord (*i.e.* chord with high-lift devices deployed), see Sketch 4.1	m	ft
c_{el}	effective chord of leading-edge device, see Table 4.1	m	ft
c_l	chord of leading-edge device, see Sketches 4.1 and 4.2	m	ft
c'_l	extended chord of leading-edge device, see Sketches 4.1 to 4.3	m	ft

Δc_l	chord extension due to deployment of leading-edge device, see Sketches 4.1 to 4.3	m	ft
F_R	factor for effect of Reynolds number on ΔC_{Lml}, Equation (3.11)		
G_l	slat or vented Krüger gap; distance between device trailing edge and aerofoil surface, normal to aerofoil surface, see Sketch 4.2(a) or 4.2(b)	m	ft
H_l	height of slat or vented Krüger flap trailing edge above aerofoil chord line, see Sketch 4.2(a) or 4.2(b)	m	ft
K_e	correlation factor for overlap of slat trailing edge, Figure 3		
K_g	correlation factor for geometry of leading-edge device, Figures 2a and 2b		
K_l	correlation factor for effect of leading-edge device deflection*, Figures 1a to1c		
K_0	correlation factor in $[\Delta C'_{L0l}]_1$, dependent on type of leading-edge device, see Table 4.1		
L_l	overlap between deployed slat or vented Krüger flap trailing-edge and fixed aerofoil nose, see Sketch 4.2(a) or 4.2(b)	m	ft
M	free-stream Mach number		
R_c	Reynolds number based on free-stream conditions and aerofoil chord c		
t	maximum thickness of aerofoil	m	ft
x	chordwise distance aft from leading edge of basic (plain) aerofoil	m	ft
x_l	chordwise location of undeployed slat trailing-edge, see Sketch 4.2(a)	m	ft
x_n	chordwise location of fixed aerofoil nose, see Sketch 4.2(a)	m	ft
x_τ	chordwise location of trailing edge, of c'_l for deployed Krüger flaps and sealed slats, see Sketch 4.3(a) to 4.3(c)	m	ft
z_h	vertical location of hinge for drooped leading edge, see Sketch 4.1	m	ft
$z_{u1.25}$	upper-surface ordinate at $x = 0.0125c$ for basic (plain) aerofoil	m	ft
δ_l, δ_l°	deflection of leading-edge device, see Sketches 4.1 to 4.3	rad, deg	rad, deg

δ_0, δ_0°	datum value of δ_l, δ_l° at which $\Delta C'_{Lml} = 0$, dependent on type of leading-edge device, see Table 4.1	rad, deg	rad, deg
θ_l	angular parameter related to effective chord of leading-edge device, Equation (3.4)	rad	rad
ρ_l	leading-edge radius of basic (plain) aerofoil or leading-edge device	m	ft

Subscripts

$(\ )_{expt}$	denotes experimental value
l	denotes leading-edge device
$(\ )_{pred}$	denotes predicted value

Superscript

$^\circ$	denotes angle in degrees
$'$	denotes value based on extended chord

* Plus other deployment effects related to deflection for other than plain leading-edge flap and drooped leading edge, see Sections 4.2 and 4.3.

2. INTRODUCTION

2.1 Scope of the Item

This Item provides semi-empirical methods for estimating the incremental effects on aerofoil lift at zero angle of attack and on maximum lift due to the deployment of various leading-edge high-lift devices at low speeds. The types of leading-edge device considered are plain flaps, drooped leading edges, slats (including sealed slats) and Krüger flaps (including vented Krügers).

Section 3 outlines the background to the development of the methods and provides the resulting equations for the estimation of ΔC_{L0l}, the increment in lift coefficient at zero angle of attack and ΔC_{Lml}, the increment in maximum lift coefficient due to the deployment of a leading-edge device.

Section 4 presents the means whereby particular types of leading-edge device are treated. For easy reference a tabular layout is used to show numerical values or the location of the data required to evaluate the equations for each of the leading-edge devices covered.

Section 5 concerns applicability and accuracy, Section 6 gives the Derivation and Reference and, finally, Section 7 presents a number of detailed examples illustrating the use of the methods.

2.2 Application of Data to Aerofoils with Trailing-edge Flaps

In order to use the data obtained from the present Item in the wider context in which trailing-edge flaps are also used, it is essential to refer to Item No. 94026 (Reference 15). That Item acts as an introduction to, and a link between, the Items in the complete series dealing with the incremental effects of high-lift device deployment on aerofoil lift at zero angle of attack and at its maximum. It describes how the incremental effects are summed and added to the contributions from the basic (*i.e.* plain) aerofoil to give the total lift coefficient values at zero angle of attack, C_{L0}, and at maximum lift, C_{Lm}.

3. LIFT COEFFICIENT INCREMENTS ΔC_{L0l} AND ΔC_{Lml}

First approximations to the lift coefficient increments due to the deployment of leading-edge high-lift devices can be obtained from the theory for an equivalent thin hinged plate with empirical correlation factors to account for the geometry of practical aerofoil high-lift devices. To make some allowance for the effects of chord extension in the theory, the flap chord ratio and the lift coefficient increments are based on the aerofoil extended chord. This approach was used in Derivation 11 and the methods developed for this Item have improved on that approach and applied it to a wider range of leading-edge devices. The resulting methods are as follows.

3.1 Increment in Lift Coefficient at Zero Angle of Attack

The deployment of a leading-edge device gives a (usually small) loss in aerofoil lift at zero angle of attack, determined from

$$\Delta C'_{L0l} = [\,\Delta C'_{L0l}\,]_1 + [\,\Delta C'_{L0l}\,]_2 \,. \tag{3.1}$$

The prime symbol $(')$ indicates that the lift coefficient increment is based on the aerofoil extended chord c'.

In Equation (3.1) the first term is the main contribution obtained from the theory, and is given by

$$[\Delta C'_{L0l}]_1 = K_0 a_l \delta_l \tag{3.2}$$

where K_0 is an empirical correlation factor, which is dependent upon the type of leading-edge device, and a_l is the theoretical rate of change of lift coefficient with respect to the deflection δ_l, positive nose down, given by thin plate theory as

$$a_l = -2(\theta_l - \sin\theta_l) \tag{3.3}$$

where
$$\theta_l = \cos^{-1}(1 - 2c_{el}/c') \tag{3.4}$$

and
$$\sin\theta_l = [1 - (1 - 2c_{el}/c')^2]^{\frac{1}{2}}, \tag{3.5}$$

in which c_{el} is the effective chord of the leading-edge device.

Combination of Equations (3.2) to (3.5) gives, in conjunction with Equation (3.1),

$$\boxed{\Delta C'_{L0l} = -2K_0\delta_l \{\, \cos^{-1}(1 - 2c_{el}/c') - [1 - (1 - 2c_{el}/c')^2]^{\frac{1}{2}}\} + [\Delta C'_{L0l}]_2 \,,} \tag{3.6}$$

in which $[\Delta C'_{L0l}]_2$ is a correction required only for slats and vented Krüger flaps.

To convert the lift coefficient based on extended chord to one based on basic aerofoil chord, the equation

$$\Delta C_{L0l} = (c'/c)\Delta C'_{L0l} \tag{3.7}$$

is used. The value of ΔC_{L0l} can be taken to be independent of Reynolds number.

The determination of $\Delta C'_{L0l}$ for various types of leading-edge device is given in Section 4.

3.2 Increment in Maximum Lift Coefficient

The increment in maximum lift coefficient is given by

$$\Delta C'_{Lml} = K_e K_g K_l a_{ml}(\delta_l - \delta_0) \tag{3.8}$$

For given flow conditions the empirical correlation factors K_e, K_g and K_l are dependent only upon leading-edge device geometry. In this Item K_e, K_g and K_l have been determined for a datum Reynolds number of $R_c = 3.5 \times 10^6$ (see Section 5). The parameter a_{ml} is the theoretical rate of change of maximum lift coefficient with respect to δ_l, given by thin plate theory as

$$a_{ml} = 2\sin\theta_l \tag{3.9}$$

in which $\sin\theta_l$ is given by Equation (3.5).

Equation (3.8) can be rewritten, using Equations (3.9) and (3.5), as

$$\boxed{\Delta C'_{Lml} = 2K_e K_g K_l(\delta_l - \delta_0)[1-(1-2c_{el}/c')^2]^{\frac{1}{2}}}, \tag{3.10}$$

for the datum Reynolds number. The parameter δ_0 is the empirically-derived value of δ_l required to give $\Delta C'_{Lml} = 0$ for slats and vented Krüger flaps.

The magnitude of ΔC_{Lml} is influenced by Reynolds number. Analysis of data in Derivations 10 and 14 showed that if K_e, K_g and K_l were correlated at a datum Reynolds number, taken here as $R_c = 3.5 \times 10^6$, then all the Reynolds number dependence of ΔC_{Lml} could be allowed for through a factor, F_R, given by

$$F_R = 0.153\log_{10} R_c, \tag{3.11}$$

which is unity at the datum.

Thus

$$\Delta C_{Lml} = F_R(c'/c)\Delta C'_{Lml}. \tag{3.12}$$

The method for the determination of $\Delta C'_{Lml}$ for various types of leading-edge device is given in Section 4.

4. DETERMINATION OF $\Delta C'_{L0l}$ AND $\Delta C'_{Lml}$ FOR A RANGE OF LEADING-EDGE HIGH-LIFT DEVICES

To determine values of $\Delta C'_{L0l}$ and $\Delta C'_{Lml}$, and thence to determine the associated values of ΔC_{L0l} and ΔC_{Lml}, for the various types of leading-edge device, Equations (3.6) and (3.10) are used in conjunction with Equations (3.7) and (3.12). The parameters involved in Equations (3.6) and (3.10) take different values according to the type of leading-edge device, so Table 4.1 is presented to show the source of the required geometry and definitions or locations whereby the relevant parameters can be determined.

TABLE 4.1 Source of geometry and relevant parameters required for evaluation of Equations (3.6) and (3.10) for various leading-edge devices

Leading-edge device	*Geometry in Section*	*Parameter in Equation (3.6) or (3.10)*							
		c_{el}	δ_l	K_0	$[\Delta C'_{L0l}]_2$	K_e	K_g	K_l	δ_0
Plain leading-edge flaps and drooped leading edges	4.1	c'_l	Sketch 4.1	$1/K_l$	0	1.0	Fig. 2a	Fig. 1a	0
Slats and vented Krüger flaps*	4.2	c_l	Sketch 4.2	1.35	0.030	Fig 3 for slats, 1.0 for vented Krügers	Fig. 2b	Fig. 1b	0.25
Krüger flaps and sealed slats*	4.3	c'_l	Sketch 4.3	1.8	0	1.0	Fig. 2a	Fig. 1c	0

* It is **essential** to refer to Section 4.3 for the determination of ΔC_{Lml} for Krüger flaps (vented or unvented) for details of a limitation on Krüger nose geometry.

In addition to the sketches, Sections 4.1 to 4.3 contain special comments concerning the geometry and its influence on $\Delta C'_{L0l}$ or $\Delta C'_{Lml}$ via the correlation parameters.

4.1 Plain Leading-edge Flaps and Drooped Leading Edges

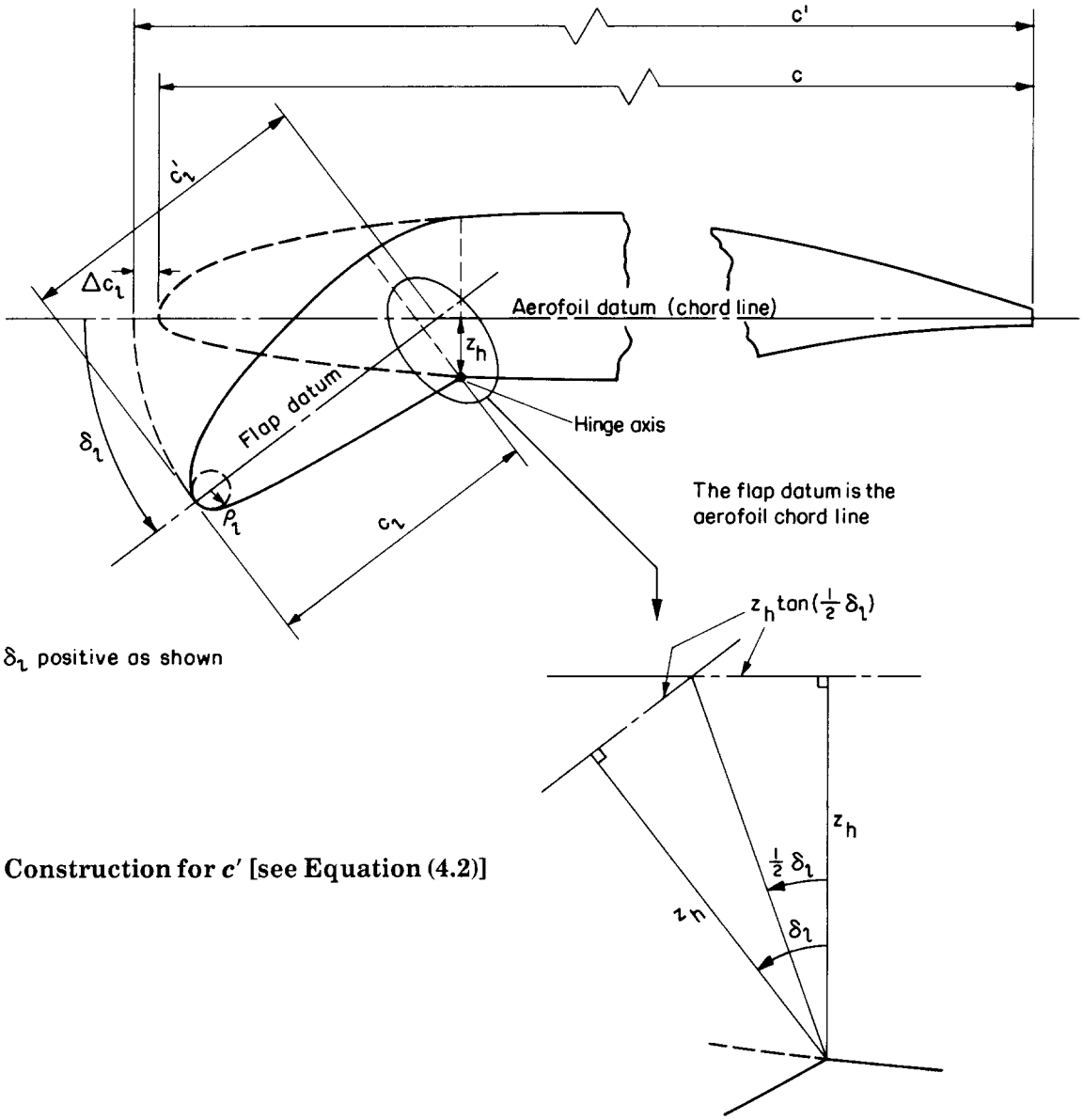

Construction for c' [see Equation (4.2)]

Sketch 4.1 Plain leading-edge flaps and drooped leading edges

From Sketch 4.1,

$$c_l' = c_l + z_h \tan(\delta_l/2) \tag{4.1}$$

and

$$c' = c + 2z_h \tan(\delta_l/2)\,. \tag{4.2}$$

Equations (4.1) and (4.2) relate to the specific type of device shown in Sketch 4.1, *i.e.* a device deployed by rotation around a lower-surface hinge. Many variations in design are possible and the corresponding values of c_l' and c' appropriate to any other arrangement used would have to be determined.

4.2 Slats and Vented Krüger Flaps

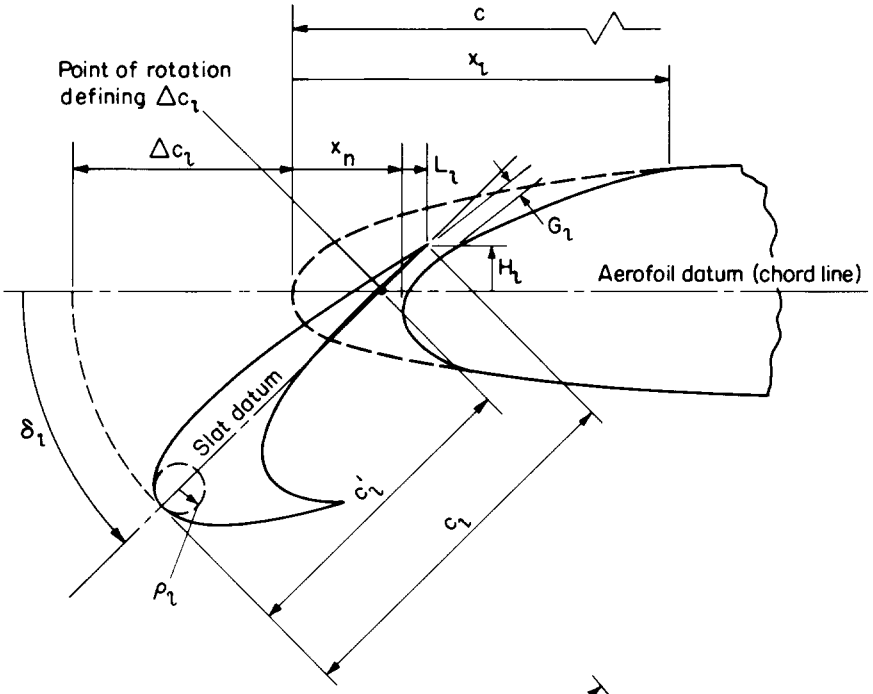

(a) Slat

δ_l, H_l and L_l positive as shown

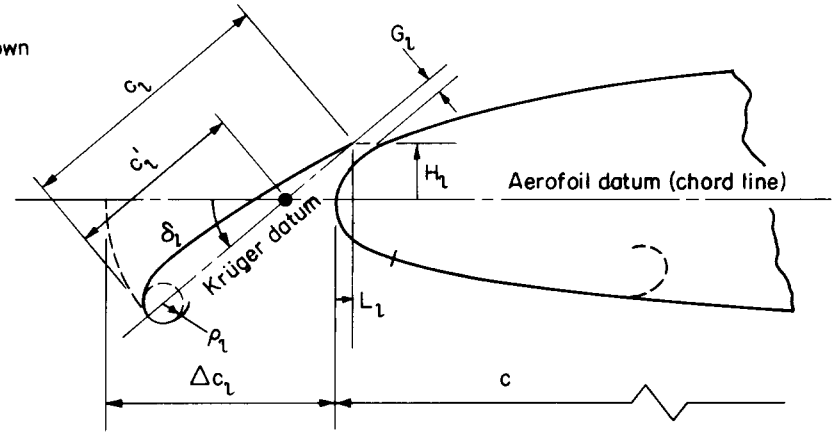

(b) Vented Krüger flap

$a = H_l \operatorname{cosec} \delta_l \tan(\frac{1}{2}\delta_l)$
$b = a \sin \delta_l$
$= H_l \tan(\frac{1}{2}\delta_l)$

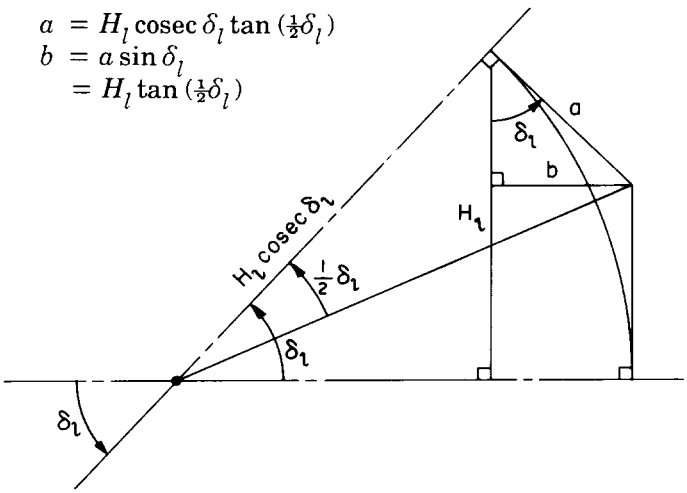

(c) Construction for c' [see Equations (4.4a) and (4.4b)]

Sketch 4.2 Slats and vented Krüger flaps

The deflection, δ_l, of both slats and vented Krüger flaps is defined using the angle between the datum chords of the slat (or flap) and the aerofoil. The slat (or flap) datum chord is defined using the line passing through the centre of the leading-edge radius and the slat trailing edge. The extended chord, c', and the chord extension, Δc_l, are defined by rotating the slat (or flap) about the intersection of the slat (or flap) and aerofoil datum chords, as shown in the sketch.

In Sketches 4.2(a) and 4.2(b), for a slat and vented Krüger flap

$$c'_l = c_l - H_l \operatorname{cosec} \delta_l . \tag{4.3}$$

For a slat, the geometry in Sketch 4.2(a) gives

$$\begin{aligned} c' &= c + \Delta c_l \\ &= c + c_l - x_n - L_l - H_l \tan(\delta_l/2) . \end{aligned} \tag{4.4a}$$

For a vented Krüger flap, the geometry in Sketch 4.2(b) gives

$$\begin{aligned} c' &= c + \Delta c_l \\ &= c + c_l - L_l - H_l \tan(\delta_l/2) . \end{aligned} \tag{4.4b}$$

Problems special to slats and vented Krüger flaps

While no test data were found for vented Krüger flaps on aerofoils the method for slats is expected to apply, but see (iii) below. With regard to the development of the prediction methods, slats presented particular problems, requiring the introduction of special correlating parameters.

(i) A bias in predicted values of $\Delta C'_{L0l}$ necessitated the introduction of a small correction, $[\Delta C'_{L0l}]_2$, see Equation (3.6).

(ii) The way in which slat deflection, δ_l, is defined required the use of what is effectively a datum value, $\delta_l = \delta_0$, at which $\Delta C'_{Lml} = 0$, see Equation (3.10).

(iii) In general, optimum slat performance occurs when the slat trailing edge is not too far removed from the leading-edge region of the fixed portion of the aerofoil. In order to take some account of the reduction in $\Delta C'_{Lml}$ that occurs when that is not the case, the factor K_e was introduced as a function of the dimensionless overlap $L_l/(x_l - x_n)$, see Figure 3. For vented Krüger flaps it is suggested that $K_e = 1$ be used, which is felt to be acceptable for the small values of L_l/c normally used for such flaps.

(iv) The correlation parameter K_l is mainly dependent upon deflection. For slats and vented Krüger flaps, however, there is a secondary effect of dimensionless gap, G_l/c, see Figure 1b. It is seen that at low values of δ_l the effect of increasing G_l/c is initially to increase K_l to a maximum of about 1.15 at $G_l/c = 0.035$ with a reduction thereafter, but see also Section 5.

(v) The method for ΔC_{Lml} for vented Krüger flaps is only applicable to those cases in which the leading-edge radius of the flap is the same as that of the basic aerofoil (see also Section 4.3).

4.3 Krüger Flaps and Sealed Slats

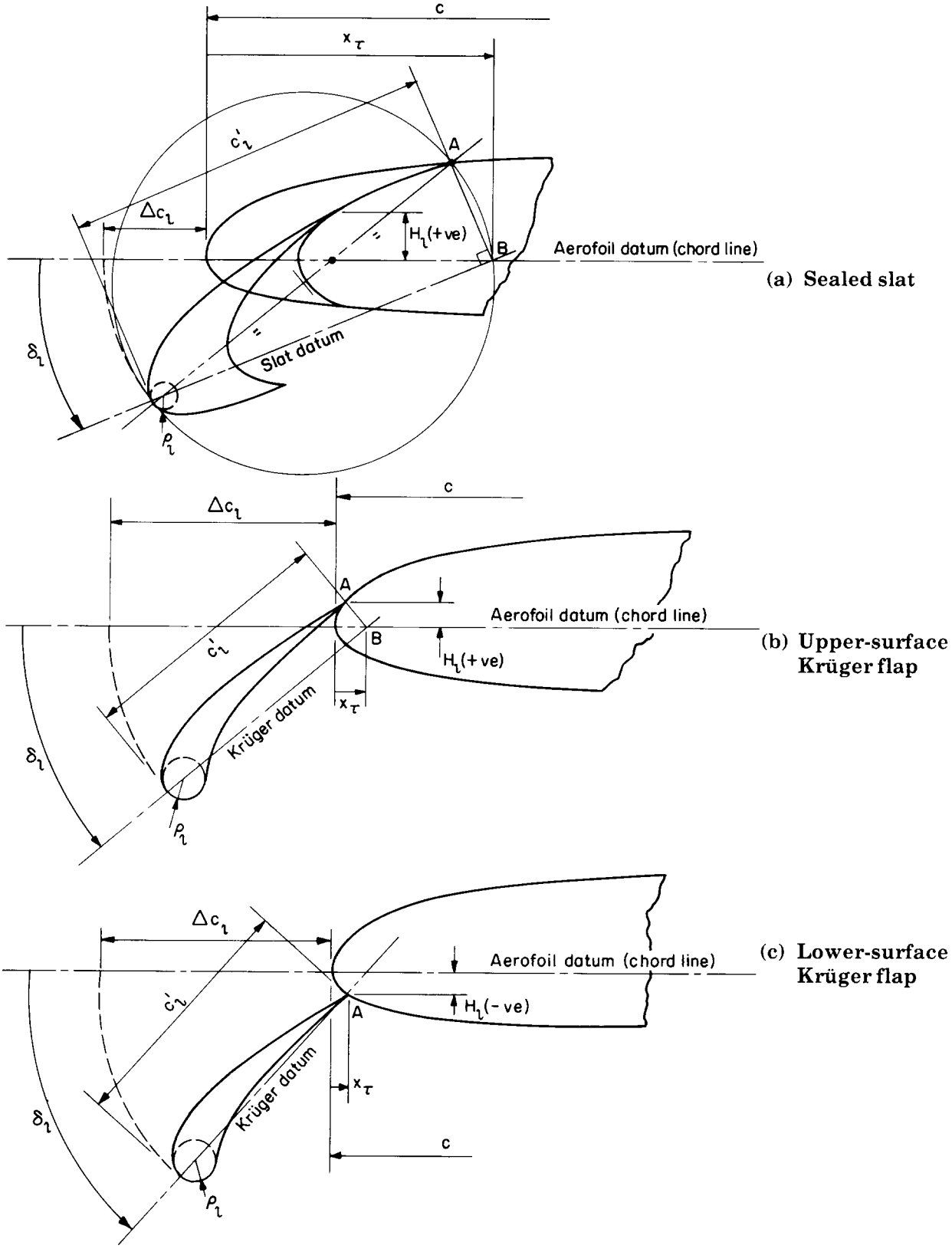

Sketch 4.3 Krüger flaps and sealed slats

Krüger flaps and sealed slats have no slot and are therefore quite similar, in terms of their operation, to plain leading-edge flaps; the methods for predicting $\Delta C'_{L0l}$ and $\Delta C'_{Lml}$ are likewise similar. The main problem is the definition of equivalent flap chord c'_l and deflection angle δ_l. Sketches 4.3(a) to 4.3(c) show how they are defined for sealed slats and two forms of Krüger flap, termed upper and lower surface Krüger flaps.

For the sealed slat and upper-surface Krüger flap the equivalent leading-edge flap is taken to be related to that part of the aerofoil and flap forward of the point at which the section first departs from the original upper-surface profile due to the deployment of the flap, *i.e.* points A on Sketches 4.3(a) and 4.3(b). The flap chord and deflection consistent with this are shown on those sketches. There is of necessity a small difference in the definitions for the case of the lower-surface Krüger flap, see Sketch 4.3(c).

Sealed slats and upper-surface Krüger flaps (Sketches 4.3(a) and 4.3(b))

For sealed slats and upper-surface Krüger flaps the values of c'_l and δ_l for the equivalent plain flap are obtained as follows. A straight line is drawn from the leading edge and passing through the centre of the flap leading-edge radius to point A, the point of departure from the original aerofoil surface. A circle centred on the mid-point of this line intersects the basic aerofoil chord at point B. The straight line joining B to the flap leading edge and passing through the centre of the flap leading-edge radius defines the equivalent plain flap chord c'_l. The angle between that chord and the aerofoil chord defines δ_l.

Lower-surface Krüger flap (Sketch 4.3(c))

For a lower-surface Krüger flap, where the flap trailing-edge is on the aerofoil lower surface, the chord c'_l is taken as the length of the line drawn from A to the leading edge of the flap, passing through the centre of the flap leading-edge radius.

In Sketches 4.3(a) to 4.3(c)

$$\begin{aligned} c' &= c + \Delta c_l \\ &= c + c'_l - x_\tau . \end{aligned} \tag{4.5}$$

The correlating parameter K_l is a function of δ_l, but for sealed slats and Krüger flaps there is also a strong dependency on the dimensionless trailing-edge height H_l/c, see Figure 1c. It will be seen that K_l rises to a maximum at $H_l/c = 0.01$ and remains at the value for $H_l = 0$ when H_l/c is negative, but see Section 5.

Effect of leading-edge radius on ΔC_{Lml} for Krüger flap

The method of Section 3 treats Krüger flaps (vented or unvented) in the same way as slats (sealed or unsealed). Slats are considered by means of an empirical adaptation of theoretical values of maximum lift increment for plain leading-edge flaps on thin plates. Consequently, the resulting plots for K_g as a function of ρ_l/c for slats were taken to apply to Krüger flaps.

However, plain leading-edge flaps and slats both have a leading-edge radius that is by definition the same as that of the aerofoil. The leading-edge radius of a Krüger flap is not necessarily the same as that of the aerofoil; indeed that is an advantage of the Krüger flap in that its nose geometry can be optimised without the risk of jeopardising the performance of the basic aerofoil.

The application to Krüger flaps of the K_g values derived for slats is therefore valid only when the Krüger flap leading-edge radius is the same as that of the aerofoil. This situation applied to the small number of test data (Derivations 3 and 5) used to confirm the application to Krüger flaps.

Lack of suitable data prevents the development of a means of treating those cases in which the leading-edge radius of the Krüger flap differs from that of the basic aerofoil. For example, Derivation 3 contains data relating to one configuration of lower-surface Krüger flap (Sketch 4.3(c)) for which the flap hinge was set well back ($x_\tau/c = 0.0225$) from the leading-edge of the aerofoil and the leading-edge radius of the flap was about 25% less than that of the aerofoil. However, there were no directly comparable test data for the same configuration but with a change of leading edge radius. The tentative indications from those tests are that a reduction in Krüger leading-edge radius leads to a reduction in the optimum value of ΔC_{Lml}, although the poor aerodynamic conditions due to the surface discontinuity at the hinge might have been significant.

5. APPLICABILITY AND ACCURACY

5.1 Applicability

The methods given in this Item for estimating the increments in aerofoil lift coefficient at zero angle of attack and in maximum lift coefficient due to the deployment of leading-edge high-lift devices are applicable to a wide range of such devices. Table 5.1 gives the ranges of parameters covered by measured data, obtained from Derivations 1 to 9 and 12, for which the various correlation factors used in developing the methods have been obtained.

TABLE 5.1 Parameter ranges for test data used in methods of Section 4

Parameter	*Plain leading-edge flaps and drooped leading edges*	*Slats and vented Krüger flaps*	*Krüger flaps and sealed slats*
t/c	0.06 to 0.10	0.09 to 0.15	0.09 to 0.15
ρ_l/c	0.004 to 0.0069	0.005 to 0.0158	0.0055 to 0.015
ρ_l/t	0.067 to 0.0687	0.055 to 0.132	0.061 to 0.10
x_n/c	Not applicable	0.0185 to 0.05	Not applicable
c_{el}/c	0.15	0.125 to 0.218	0.097 to 0.306
$\delta_l°$ (undeflected)	Not applicable	13° to 27°	Not applicable
$\delta_l°$	0 to 45°	12° to 50°	12° to 92°
L_l/c	Not applicable	–0.028 to 0.125	Not applicable
H_l/c	Not applicable	–0.020 to 0.088	–0.0204 to 0.045
G_l/c	Not applicable	0.01 to 0.06	Not applicable
x_τ/c	Not applicable	Not applicable	0.02 to 0.25
$R_c \times 10^{-6}$	4.5 to 6.0	0.60 to 6.0	0.8 to 6.0
M	0.15 to 0.17	0.10 to 0.17	0.11 to 0.17

The methods are based on the theoretical effects derived from simple thin hinged-plate theory with empirical corrections for the effects of practical leading-edge device geometry. The leading-edge device requiring the largest number of such corrections is the slat (including the vented Krüger flap). That is not surprising since it is the device farthest removed from a simple hinged plate in terms of the physical processes involved in its operation. The slot is very influential in its own right; in the extreme case a slat can provide a change in maximum lift simply by translation, with no rotation, to open up a slot.

The method developed in this Item applies to slats in which the slot is convergent for the full length from entry to exit. A slat with a parallel slot will marginally under-perform in relation to the estimate but a divergent slot will grossly under-perform. The method applies to design and off-design deployment settings (in terms of the slat deflection, trailing-edge overlap and gap) as long as the slot is convergent. Careful optimisation could reasonably be expected to improve on the predicted value of $\Delta C'_{Lml}$, with a possible shift towards the edge of the scatter band on the accuracy plot, see Section 5.2. However, optimisation is dependent upon many factors, the effects of which cannot be generalised in a simple prediction method.

The method for predicting ΔC_{Lml} due to Krüger flaps (vented or unvented) is applicable only to those cases in which the leading-edge radius of the flap is the same as that of the basic aerofoil (see Section 4.3).

The value $R_c = 3.5 \times 10^6$ was used as the datum from which to develop the factor F_R applicable to the increment in maximum lift coefficient, see Section 3.2. Most of the data were at or around this value. The effect of Reynolds number on ΔC_{L0l} over the ranges given in Table 5.1 and for higher Reynolds numbers can be assumed to be negligible.

The method of the Item takes no account of Mach number in the increments in maximum lift coefficient due to the deployment of high-lift devices. This is not because such effects are felt to be insignificant, since even at quite low free-stream Mach numbers the local flow around a leading-edge device can attain supersonic velocities. Rather, it is due to the lack of data for Mach numbers greater than 0.17 for the types of high-lift device considered. The use of the Item is therefore restricted to $M \leq 0.2$.

5.2 Accuracy

Sketch 5.1 shows the comparison between predicted and experimental values of the increment in lift coefficient at zero angle of attack due to the deployment of various leading-edge high-lift devices. The experimental data were obtained from Derivations 1, 3 to 5, 8 and 12. With very few exceptions the predicted and test data for ΔC_{L0l} are correlated within ± 0.07.

Similarly, Sketch 5.2 presents the corresponding comparison for values of the increment in maximum lift coefficient, with experimental data being obtained from Derivations 1 to 9 and 12. With very few exceptions, the data for ΔC_{Lml} are correlated within ± 0.1.

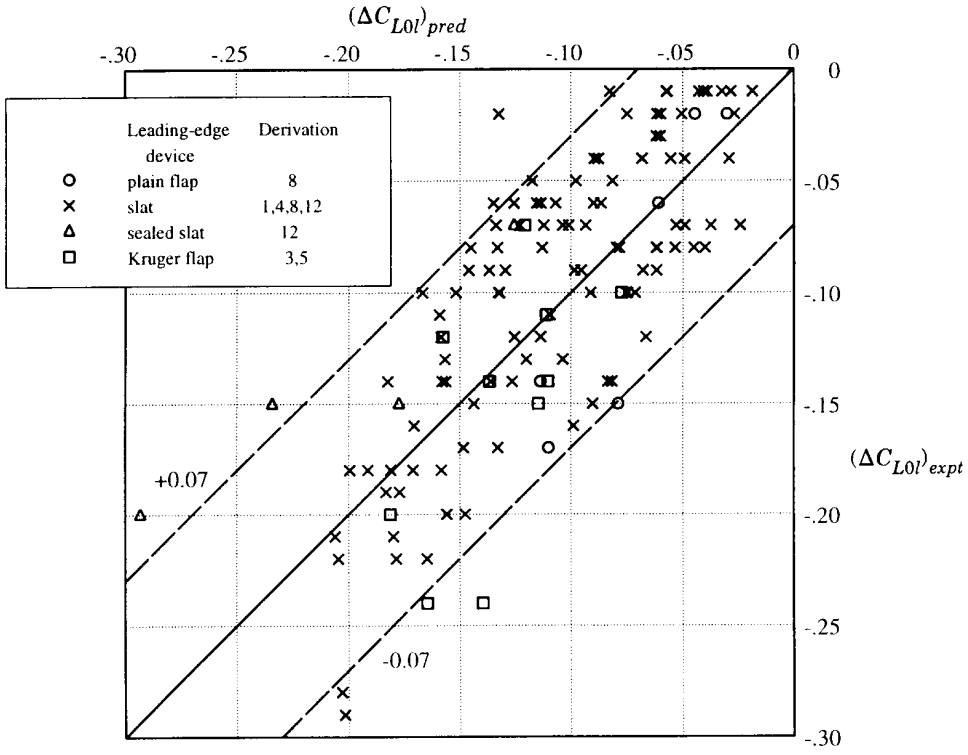

Sketch 5.1 Comparison of predicted and experimental values of ΔC_{L0l}

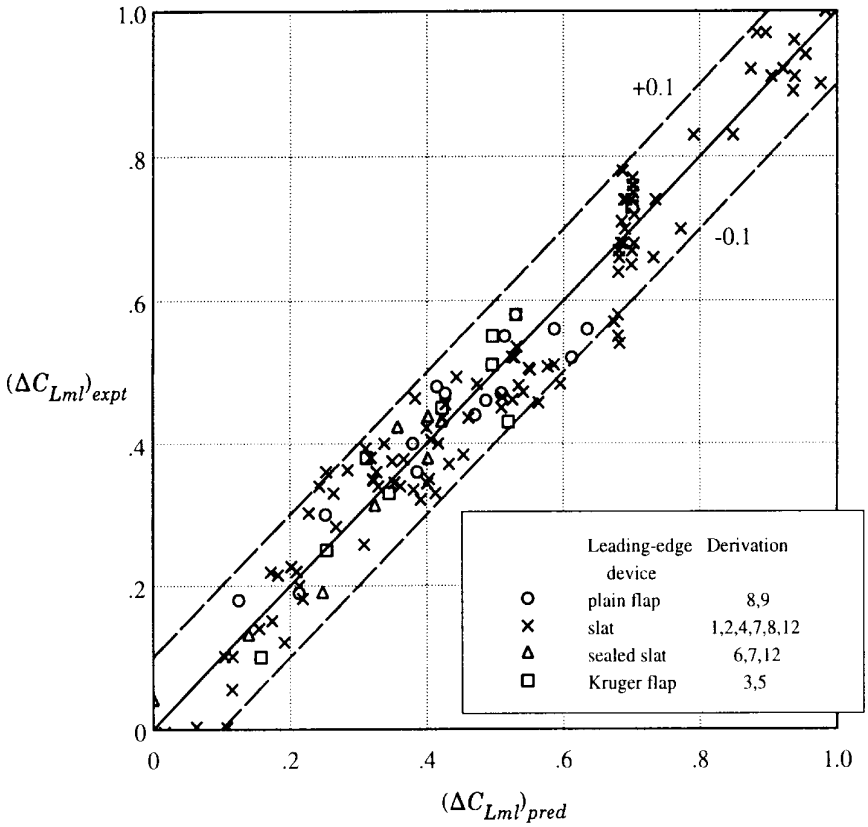

Sketch 5.2 Comparison of predicted and experimental values of ΔC_{Lml}

6. DERIVATION AND REFERENCE

6.1 Derivation

The Derivation lists selected sources of information that have assisted in the preparation of this Item.

1. WENZINGER, J.C.
   SHORTAL, J.A.
   The aerodynamic characteristics of a slotted Clark Y wing as affected by the auxiliary airfoil position.
   NACA Rep. 400, 1931.

2. BAMBER, M.J.
   Wind tunnel tests of several forms of fixed wing slot in combination with a slotted flap on an NACA 23012 airfoil.
   NACA tech. Note 702, 1939.

3. FULLMER, F.F.
   Two-dimensional wind-tunnel investigation of an NACA 64-012 airfoil equipped with two types of leading-edge flap.
   NACA tech. Note 1277, 1947.

4. QUINN, J.H.
   Test of the NACA 64_1A212 airfoil section with a slat, a double-slotted flap and boundary layer control by suction.
   NACA tech. Note 1293, 1947.

5. FULLMER, F.F.
   Two-dimensional wind-tunnel investigation of an NACA 64-009 airfoil equipped with two types of leading-edge flap.
   NACA tech. Note 1624, 1948.

6. MOSS, G.F.
   Systematic wind-tunnel tests on a 10 per cent thick symmetrical wing section (EQ 1040 profile).
   ARC R & M 2705, 1948.

7. GOTTLIEB, S.M.
   Two-dimensional wind-tunnel investigation of two NACA series airfoils with leading-edge slats.
   NACA RM L8K22 (TIL 1891), 1949.

8. KELLY, J.A.
   HAYTER, N.-L.F.
   Lift and pitching moment at low speeds of the NACA 64A010 airfoil section equipped with various combinations of a leading-edge slat, leading-edge flap, split flap and double-slotted flap.
   NACA tech. Note 3007, 1953.

9. GAINBUCCI, B.J.
   Section characteristics of the NACA 0006 airfoil with leading-edge and trailing-edge flaps.
   NACA tech. Note 3797, 1956.

10. THAIN, J.A.
    Reynolds number effects at low speeds on the maximum lift of two-dimensional aerofoil sections equipped with mechanical high lift devices.
    NAE (Div. Mech. Engng.) *Quarterly Bulletin* No. 3, 1973.

11. SCHEMENSKY, R.T.
    Development of an empirically based computer program to predict the aerodynamic characteristics of aircraft. Volume 1: Empirical methods.
    Convair Aerospace Division, General Dynamics Corporation.
    AFFDL TR-73-144 (AD 780 100), 1973.

12. LJUNGSTROM, B.L.G.
    Two-dimensional wind-tunnel experiments with single and double slotted flaps.
    Aeronaut. Res. Inst. Sweden. FFA AU-1083, 1975.

13. ESDU — Aerofoil maximum lift coefficient for Mach numbers up to 0.4. ESDU International, Item No. 84026, 1984.

14. BAe, Hatfield — Unpublished wind-tunnel test data, 1985.

6.2 Reference

The Reference contains information supplementary to that given in this Item.

15. ESDU — Introduction to the estimation of the lift coefficients at zero angle of attack and at maximum lift for aerofoils with high-lift devices at low speeds. ESDU International, Item No. 94026, 1994.

7. EXAMPLES

7.1 Example 1: Drooped Leading Edge

The incremental effects on the lift coefficient at zero angle of attack and on the maximum lift coefficient are to be estimated for the addition of 20° of leading-edge droop to a NACA 0006 aerofoil as shown in Sketch 7.1. The relevant geometrical data are

Aerofoil:	Nose droop:
$t/c = 0.06$	$c_l = 0.675$ ft $(0.15c)$
$c = 4.5$ft	$\delta_l^\circ = 20^\circ (\delta_l = 0.349$ rad.)
$\rho_l/c = 0.004$	$z_h = 0.120$ ft.

The flow conditions are

M = 0.2 and $R_c = 4.5 \times 10^6$

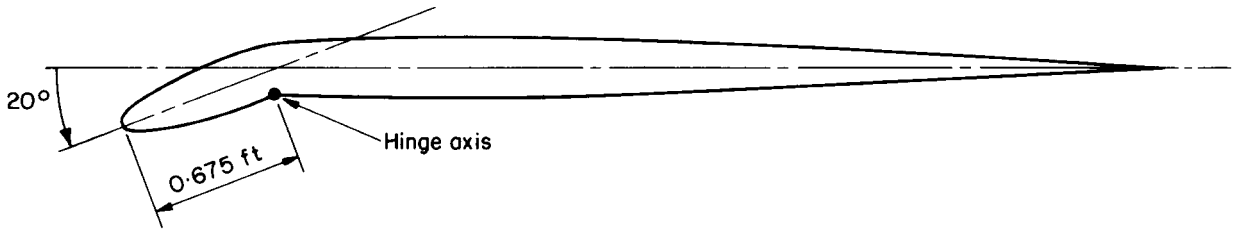

Sketch 7.1

Table 4.1 shows that Section 4.1 gives the relevant description of the geometry for a drooped leading edge. The table also shows that the value of c_{el} is taken as c_l', given by Equation (4.1) for a design having a lower-surface hinge, *i.e.*

$$c_{el} = c_l' = c_l + z_h \tan(\delta_l/2)$$
$$= 0.675 + 0.120 \times \tan(0.349/2)$$

i.e. $c_{el} = 0.696$ ft.

Also, c' is given by Equation (4.2), *i.e.*

$$c' = c + 2z_{lh}\tan(\delta_l/2)$$

$$= 4.5 + 2 \times 0.120 \times \tan(0.349/2)$$

$$= 4.542 \text{ ft.}$$

Therefore,

$$c_{el}/c' = 0.696/4.542 = 0.153$$

and $c'/c = 4.542/4.5 = 1.009.$

Table 4.1 also gives the location, or value, of all the other parameters required to evaluate Equations (3.6) and (3.10) for $\Delta C'_{L0l}$ and $\Delta C'_{Lml}$. The values of the parameters are

$$[\Delta C'_{L0l}]_2 = 0, \; K_e = 1 \text{ and } \delta_0 = 0.$$

Figure 1a gives

$$K_l = 1 \text{ for } \delta_l^\circ = 20^\circ,$$

so that $K_0 = 1/K_l = 1$ also.

Finally, Figure 2a gives $K_g = 0.82$ for $\rho_l/c = 0.004$.

Equation (3.6) for $\Delta C'_{L0l}$ now gives

$$\Delta C'_{L0l} = -2K_0\delta_l\left\{\cos^{-1}(1-2c_{el}/c') - [1-(1-2c_{el}/c')^2]^{\frac{1}{2}}\right\} + [\Delta C'_{L0l}]_2$$

$$= -2\times1\times0.349\left\{\cos^{-1}(1-2\times0.153) - [1-(1-2\times0.153)^2]^{\frac{1}{2}}\right\} + 0$$

$$= -0.058,$$

so that, from Equation (3.7),

$$\begin{aligned}\Delta C_{L0l} &= (c'/c)\Delta C'_{L0l} \\ &= 1.009 \times (-0.058) \\ &= -0.059 \approx -0.06 .\end{aligned}$$

Equation (3.10) for $\Delta C'_{Lml}$ gives

$$\begin{aligned}\Delta C'_{Lml} &= 2K_e K_g K_l(\delta_l - \delta_0)[1 - (1 - 2c_{el}/c')^2]^{½} \\ &= 2 \times 1 \times 0.82 \times 1 \times (0.349 - 0) \times [1 - (1 - 2 \times 0.153)^2]^{½} \\ &= 0.412 .\end{aligned}$$

Equation (3.11) gives, for $R_c = 4.5 \times 10^6$,

$$\begin{aligned}F_R &= 0.153 \log_{10} R_c \\ &= 0.153 \times \log_{10}(4.5 \times 10^6) \\ &= 1.018 .\end{aligned}$$

Therefore, Equation (3.12) gives

$$\begin{aligned}\Delta C_{Lml} &= F_R(c'/c)\Delta C'_{Lml} \\ &= 1.018 \times 1.009 \times 0.412 \\ &= 0.423 \approx (0.42) .\end{aligned}$$

7.2 Example 2: Leading-edge Slat

Calculate the incremental effects on the lift coefficient at zero angle of attack and on maximum lift coefficient for the aerofoil in Example 1 fitted with a slat of $c_l = 0.15c$ as shown in Sketch 7.2. The relevant geometrical data are

$$\begin{aligned} c &= 4.5 \text{ ft} & \rho_l/c &= 0.004 \\ c_l &= 0.675 \text{ ft} & H_l &= 0.054 \text{ ft} \\ \delta_l^\circ &= 30.5^\circ \ (\delta_l = 0.532 \text{rad.}) & G_l &= 0.054 \text{ ft} \\ x_n &= 0.135 \text{ ft} & L_l &= 0.030 \text{ ft} \\ x_l &= 0.666 \text{ ft} \end{aligned}$$

The flow conditions are $M = 0.2$, $R_c = 4.5 \times 10^6$.

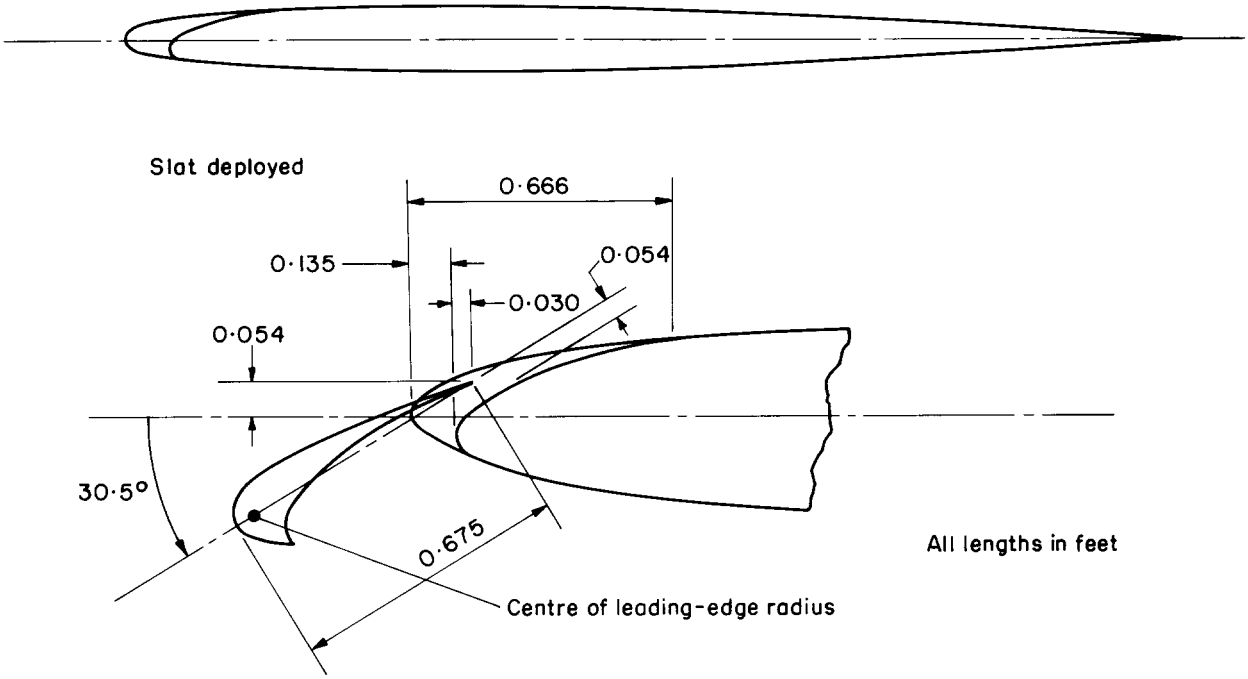

Sketch 7.2

Table 4.1 shows that Section 4.2 is the relevant section giving the geometry for a slat. The table also shows that the value of c_{el} is taken as c_l for a slat, *i.e.*

$$c_{el} = c_l = 0.675\text{ft}\,.$$

Equation (4.4a) gives the extended chord of an aerofoil with a slat as

$$\begin{aligned} c' &= c + c_l - x_n - L_l - H_l \tan(\delta_l/2) \\ &= 4.5 + 0.675 - 0.135 - 0.030 - 0.054 \times \tan(0.532/2) \\ &= 4.995\text{ ft}, \end{aligned}$$

giving $c_{el}/c' = 0.675/4.995$

$= 0.135$

and $c'/c = 4.995/4.5$

$= 1.110\,.$

Table 4.1 gives $K_0 = 1.35$, $[\Delta C'_{L0l}]_2 = 0.030$ and $\delta_0 = 0.25$

The remaining parameters, K_e, K_g and K_l, required to evaluate Equation (3.10) are given by Figures 3, 2b and 1b.

Figure 3, with a slat dimensionless overlap of

$$\begin{aligned} L_l/(x_l - x_n) &= 0.030/(0.666 - 0.135) \\ &= 0.056, \end{aligned}$$

gives $K_e = 1.$

Figure 2b, with $\rho_l/c = 0.004$, gives

$$K_g = 1.29,$$

and Figure 1b, with $\delta_l° = 30.5°$ and $G_l/c = 0.054/4.5 = 0.012$, gives

$$K_l = 0.96.$$

Equation (3.6) gives

$$\begin{aligned}\Delta C'_{L0l} &= -2K_0\delta_l\{\cos^{-1}(1-2c_{el}/c') - [1-(1-2c_{el}/c')^2]^{½}\} + [\Delta C'_{L0l}]_2 \\ &= -2\times 1.35\times 0.532\times\{\cos^{-1}(1-2\times 0.135) - [1-(1-2\times 0.135)^2]^{½}\} + 0.030 \\ &= -0.069.\end{aligned}$$

Equation (3.7) therefore gives

$$\begin{aligned}\Delta C_{L0l} &= (c'/c)\Delta C'_{L0l} \\ &= 1.110\times(-0.069) \\ &= -0.077 = -0.08.\end{aligned}$$

Equation (3.10) gives

$$\begin{aligned}\Delta C'_{Lml} &= 2K_eK_gK_l(\delta_l-\delta_0)[1-(1-2c_{el}/c')^2]^{½} \\ &= 2\times 1\times 1.29\times 0.96\times(0.532-0.25)\times[1-(1-2\times 0.135)^2]^{½} \\ &= 0.477.\end{aligned}$$

Therefore Equation (3.12) gives, with $F_R = 1.018$ from Example 1,

$$\begin{aligned}\Delta C_{Lml} &= F_R(c'/c)\Delta C'_{Lml} \\ &= 1.018\times 1.110\times 0.477 \\ &= 0.539 \approx 0.54.\end{aligned}$$

7.3 Example 3: Krüger Flap

Calculate the effect on the maximum lift coefficient of a NACA 65_2–015 section due to the deployment of a Krüger flap, shown in Sketch 7.3. The Krüger flap in this instance is an "upper-surface" type with a leading-edge radius equal to that of the aerofoil*. The geometry for the aerofoil and flap are as follows.

Aerofoil:	Krüger flap:
$t/c = 0.15$	$c'_l = 0.45$ ft
$c = 4.5$ ft	$\delta^\circ_l = 38°$ ($\delta_l = 0.663$ rad.)
	$\rho_l / c = 0.015$
	$H_l = 0.045$ ft
	$x_\tau = 0.054$ ft

The flow conditions are

$$M = 0.1 \text{ and } R_c = 4.5 \times 10^6 .$$

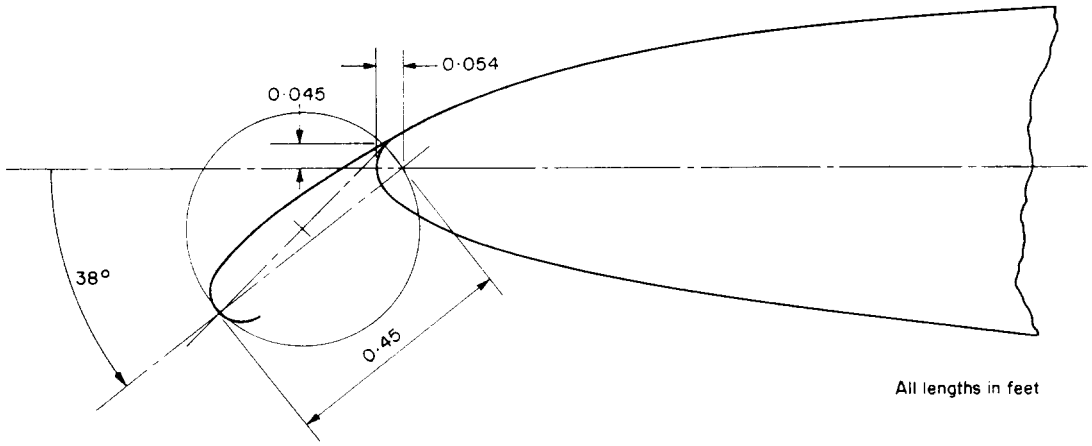

Sketch 7.3

Table 4.1 shows that Section 4.3 gives the geometry definitions for Krüger flaps without venting; Sketch 4.3(b) is appropriate to upper-surface Krüger flaps. Table 4.1 shows that $c_{el} = c'_l = 0.45$ ft in this instance. Equation (4.5) gives the extended chord as

$$\begin{aligned} c' &= c + c'_l - x_\tau \\ &= 4.5 + 0.45 - 0.054 \\ &= 4.896 \text{ ft,} \end{aligned}$$

so that

$$\begin{aligned} c_{el}/c' &= 0.45/4.896 \\ &= 0.092 \end{aligned}$$

* The method of this Item is not applicable to cases in which the leading-edge radius of the Krüger flap is different from that of the aerofoil, see Section 4.3.

and $c'/c = 4.896/4.5 = 1.088$.

Now Table 4.1 gives values of

$$K_e = 1.0 \text{ and } \delta_0 = 0\,.$$

Figure 2a gives, for $\rho_l/c = 0.015$,

$$K_g = 0.93$$

and Figure 1c, with $\delta_l^\circ = 38^\circ$ and $H_l/c = 0.045/4.5 = 0.01$,

$$K_l = 0.895.$$

Equation (3.10) therefore gives, for a Krüger flap,

$$\begin{aligned}\Delta C'_{Lml} &= 2K_eK_gK_l(\delta_l - \delta_0)[1 - (1 - 2c_{el}/c')^2]^{\frac{1}{2}} \\ &= 2 \times 1 \times 0.93 \times 0.895 \times (0.663 - 0) \times [1 - (1 - 2 \times 0.092)^2]^{\frac{1}{2}} \\ &= 0.638\,.\end{aligned}$$

From Equation (3.11), for $R_c = 4.5 \times 10^6$

$$F_R = 1.018\,,$$

as in Example 1, so that Equation (3.12) then gives, for a Krüger flap,

$$\begin{aligned}\Delta C_{Lml} &= F_R(c'/c)\Delta C'_{Lml} \\ &= 1.018 \times 1.088 \times 0.638 \\ &= 0.707 \approx 0.71\,.\end{aligned}$$

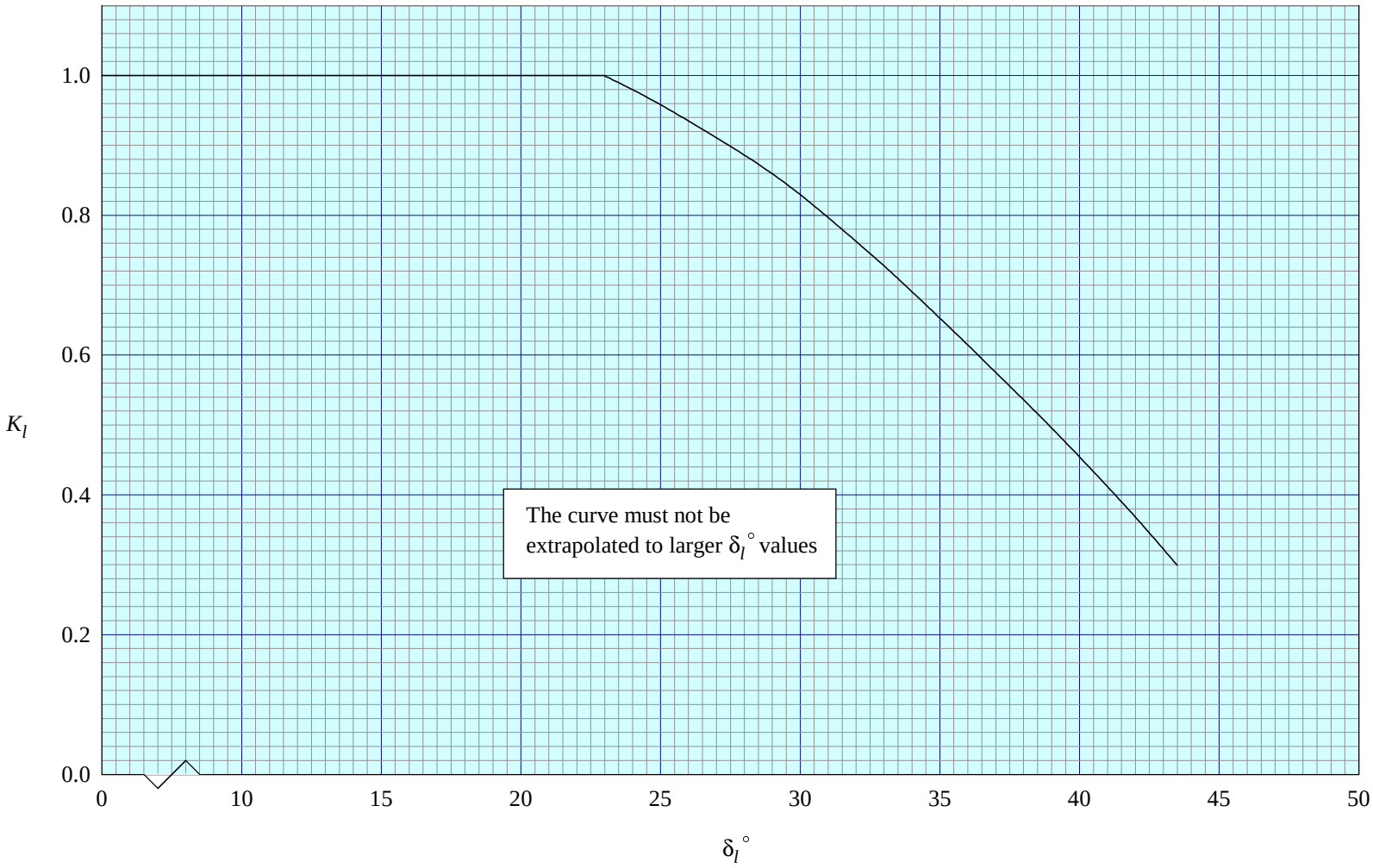

FIGURE 1a CORRELATION FACTOR K_l – Plain leading-edge flaps and drooped leading edges

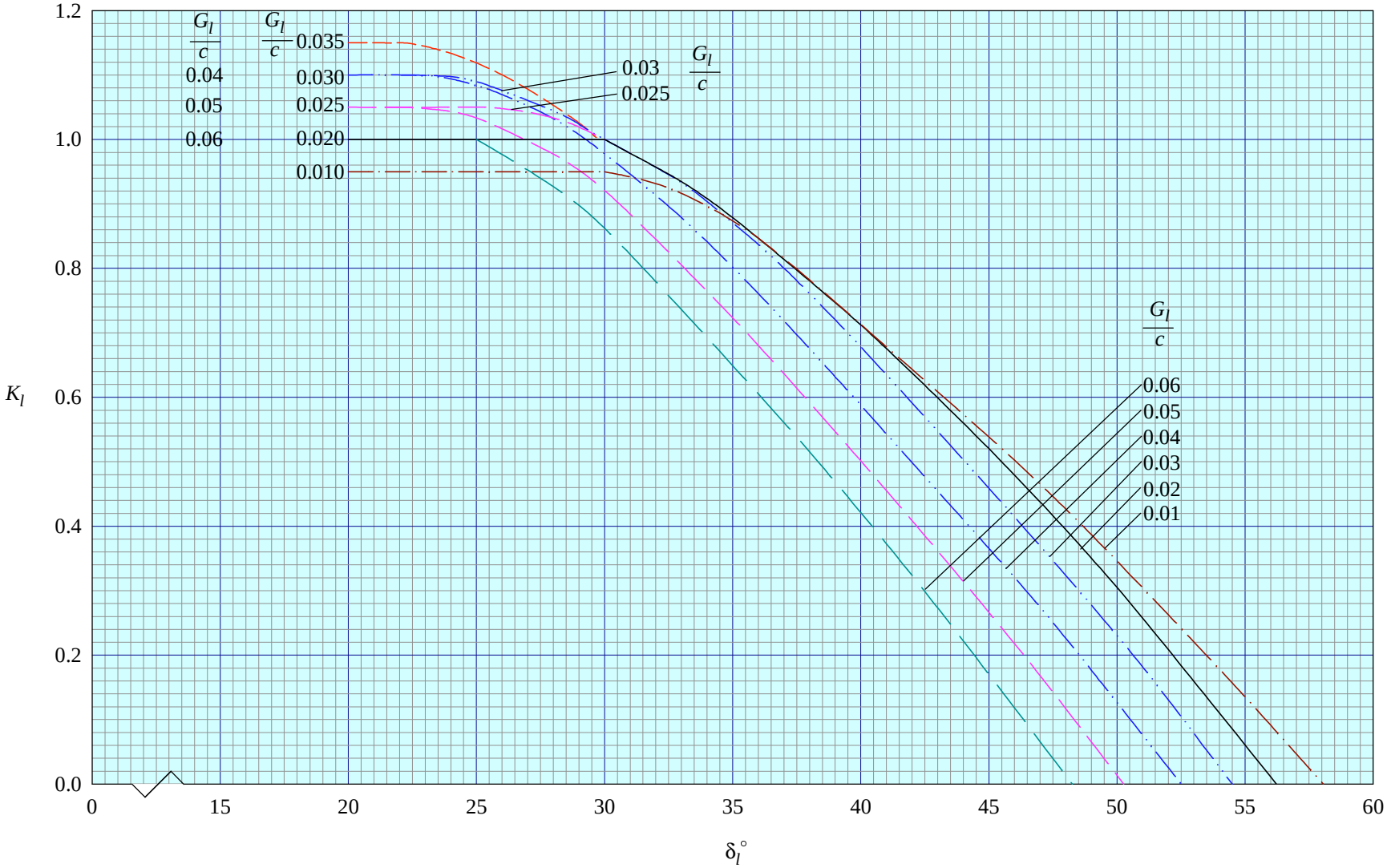

FIGURE 1b CORRELATION FACTOR K_l – Slats and vented Krüger flaps

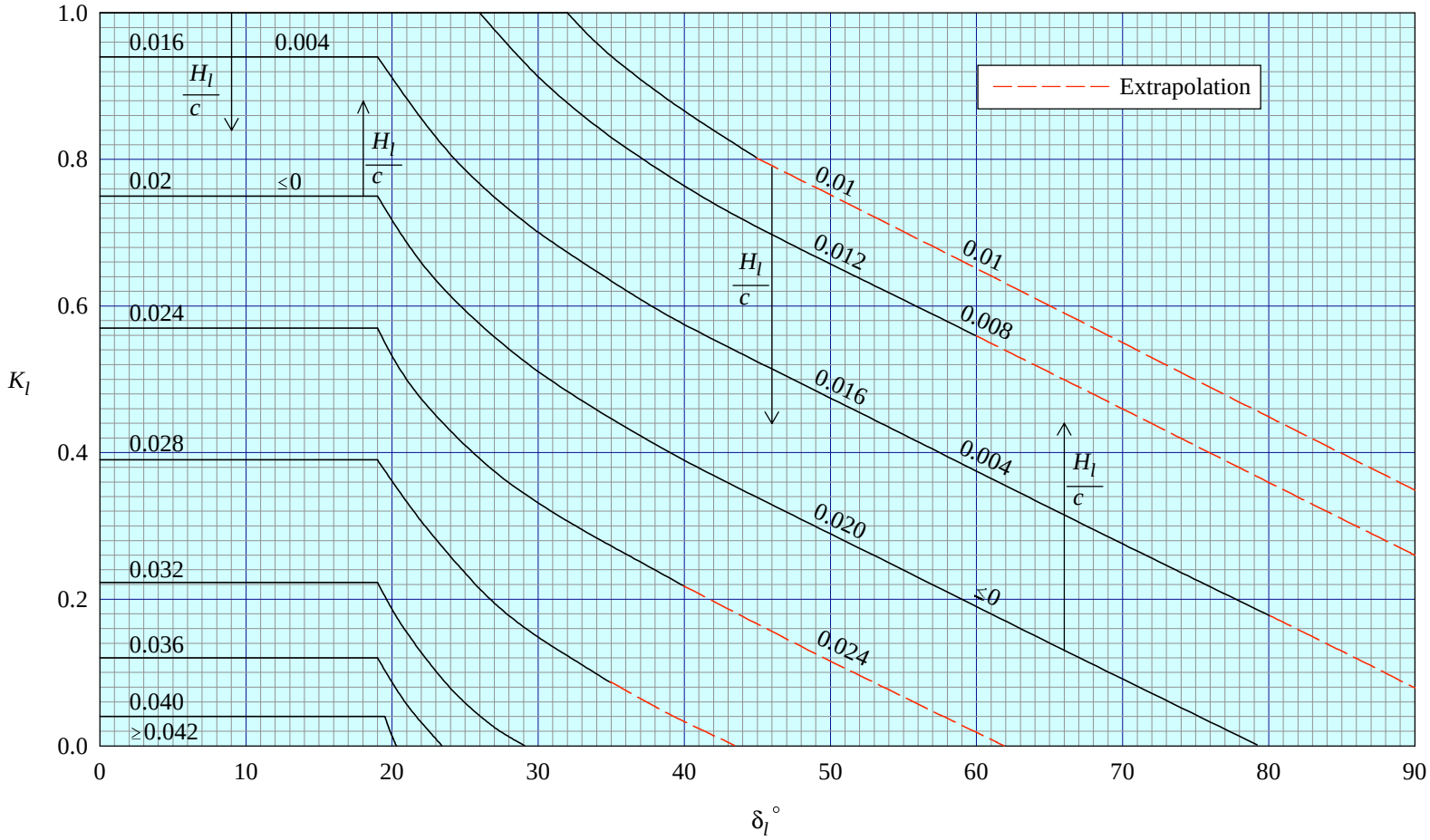

FIGURE 1c CORRELATION FACTOR K_l – Krüger flaps and sealed slats

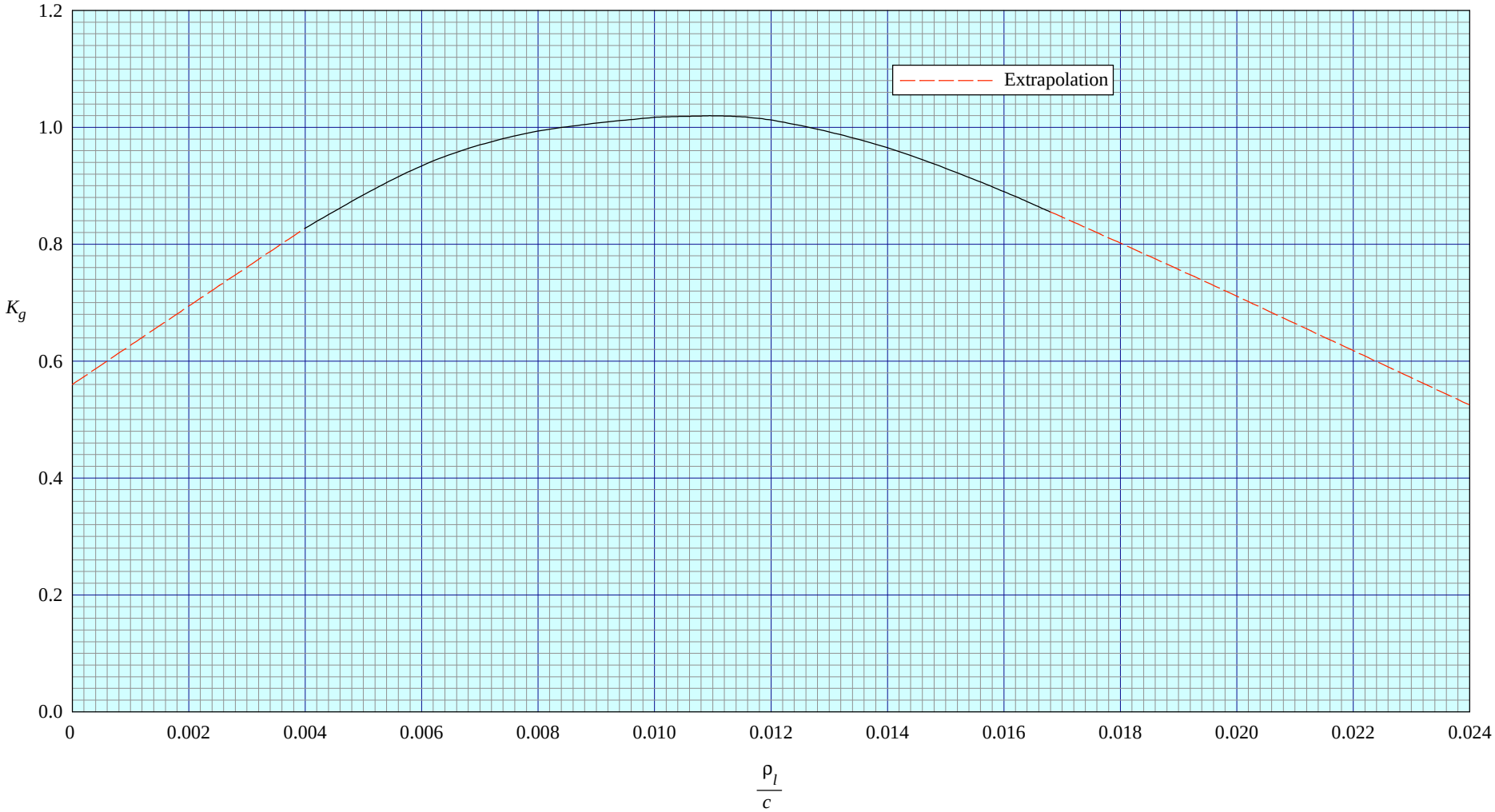

FIGURE 2a CORRELATION FACTOR K_g – Leading-edge flaps, drooped leading edges, Krüger flaps and sealed slats

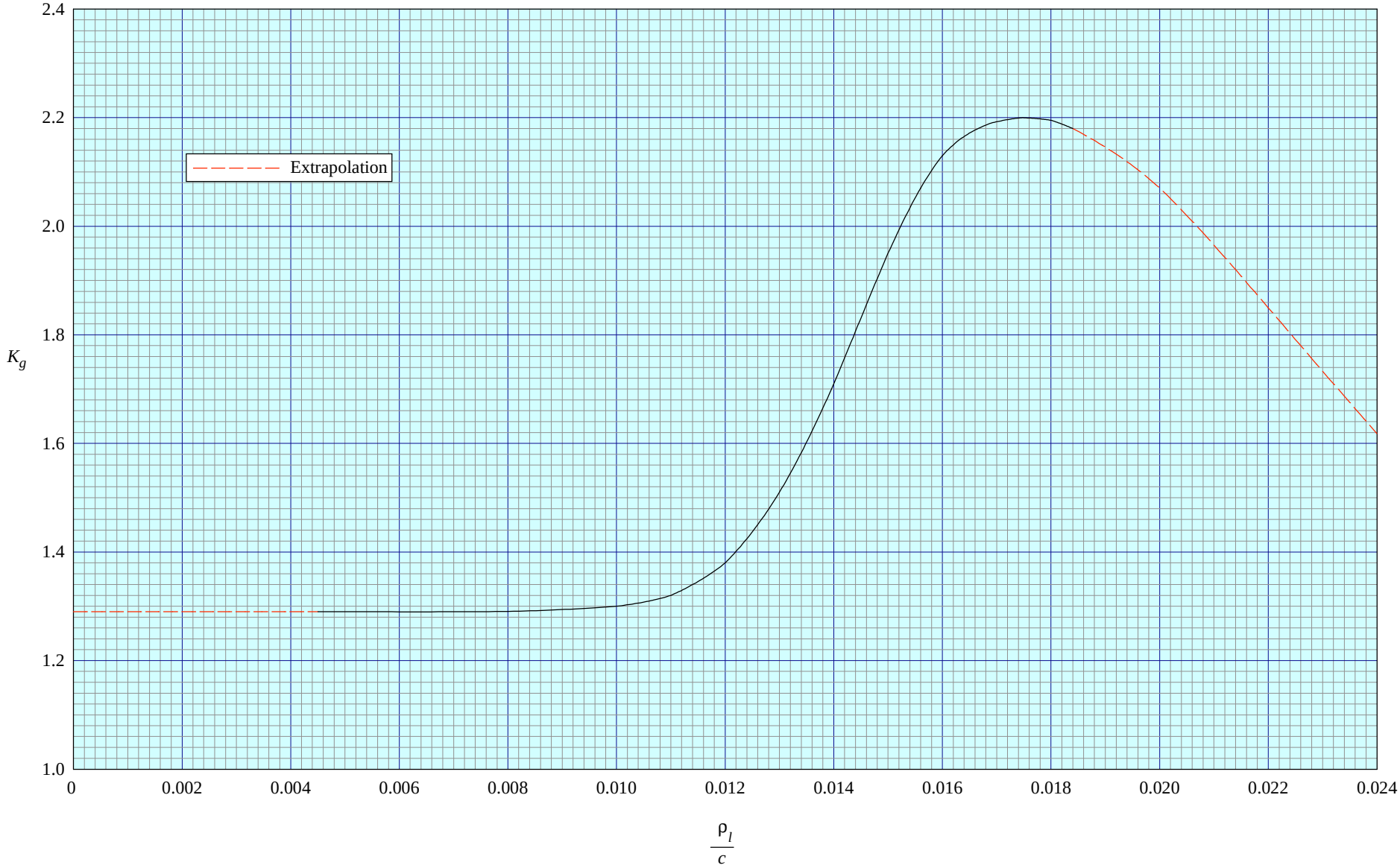

FIGURE 2b CORRELATION FACTOR K_g – Slats and vented Krüger flaps

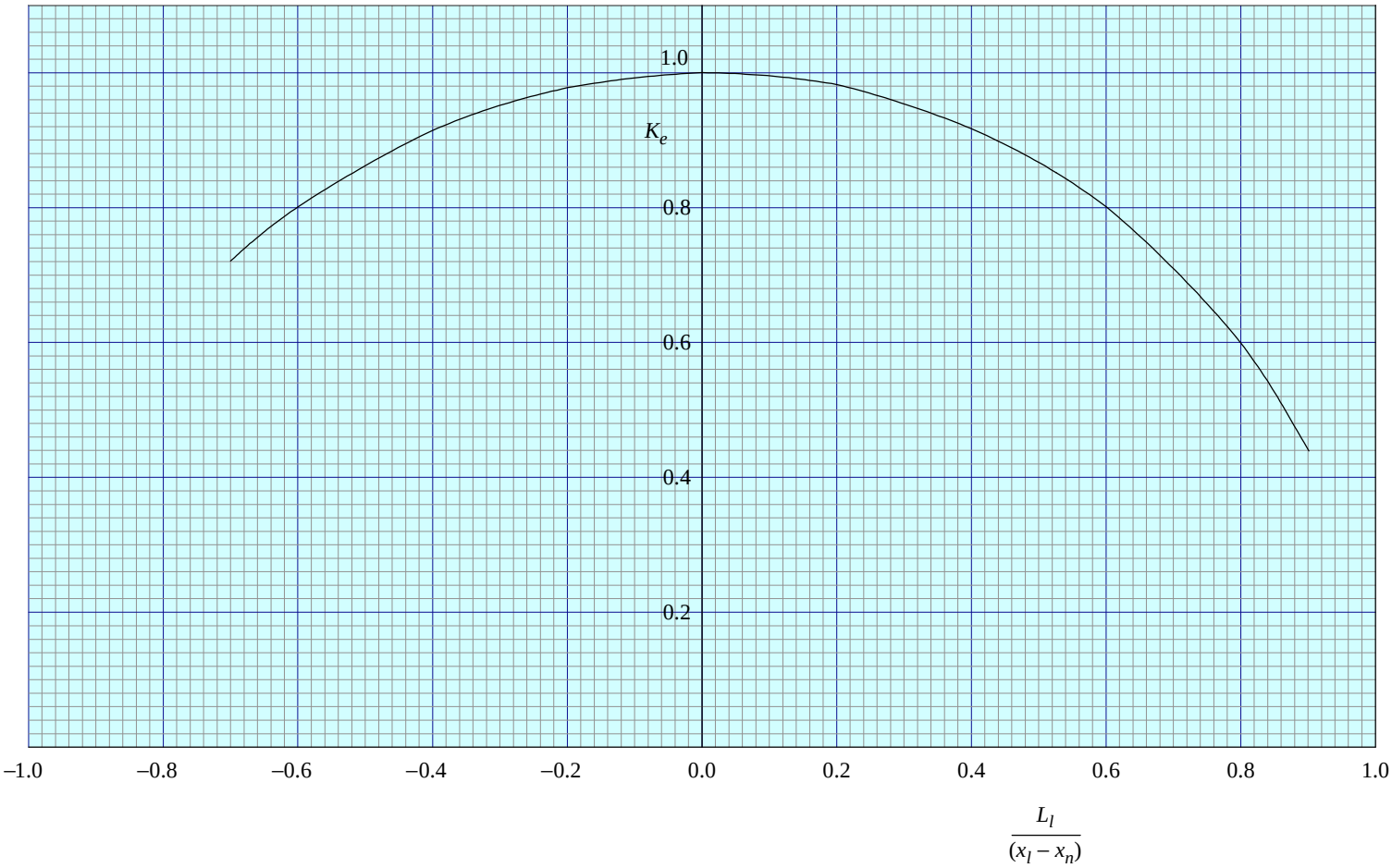

FIGURE 3 CORRELATION FACTOR K_e

THE PREPARATION OF THIS DATA ITEM

The work on this particular Item, which supersedes, in part, Item No. 85033, was monitored and guided by the Aerodynamics Committee which first met in 1942 and now has the following membership:

Chairman

Mr H.C. Garner	–	Independent

Members

Mr G.E. Bean*	–	Boeing Commercial Airplane Company, Seattle, Wash., USA
Dr N.T. Birch	–	Rolls-Royce plc, Derby
Mr D. Choo*	–	Northrop Corporation, Pico Rivera, Calif., USA
Dr P.C. Dexter	–	British Aerospace plc, Sowerby Research Centre, Bristol
Mr J.R.J. Dovey	–	Independent
Dr K.P. Garry	–	Cranfield University
Dr H.P. Horton	–	Queen Mary and Westfield College, University of London
Mr P.K. Jones	–	Independent
Mr R. Jordan	–	Independent
Mr K. Karling*	–	Saab-Scania, Linköping, Sweden
Mr M. Maurel	–	Aérospatiale, Toulouse, France
Mr J.B. Newton	–	British Aerospace Defence Ltd, Warton
Mr R. Sanderson	–	Deutsche Aerospace Airbus, Bremen, Germany
Mr A.E. Sewell*	–	McDonnell Douglas, Long Beach, Calif., USA
Mr M.R. Smith	–	British Aerospace Airbus Ltd, Bristol.

* Corresponding Member

The technical work in the assessment of the available information and the construction and subsequent development of the Data Item was carried out under contract by Mr J.R.J. Dovey.